IEEE Photonics Journal
An IEEE Photonics Society Publication

Open Access

Taper Embedded Phase-Shifted Fiber Bragg Grating Fabricated by Femtosecond Laser Line-by-Line Inscription

Volume 9, Number 6, December 2017

Feng Zhu
Zhe Zhang
Changrui Liao
Ying Wang
Lei Xu
Jun He
Chao Wang
Zhengyong Li
Tianhang Yang
Yiping Wang, *Senior Member, IEEE*

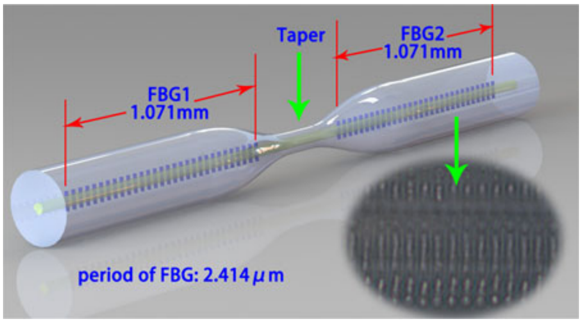

DOI: 10.1109/JPHOT.2017.2780271

Taper Embedded Phase-Shifted Fiber Bragg Grating Fabricated by Femtosecond Laser Line-by-Line Inscription

Feng Zhu,[1] Zhe Zhang,[1] Changrui Liao,[1] Ying Wang,[1] Lei Xu,[2] Jun He,[1] Chao Wang,[1] Zhengyong Li,[1] Tianhang Yang,[1] and Yiping Wang,[1] *Senior Member, IEEE*

[1]Key Laboratory of Optoelectronic Devices and Systems of Ministry of Education and Guangdong Province, College of Optoelectronic Engineering, Shenzhen University, Shenzhen 518060, China
[2]School of Electronic and Communication Engineering, Shenzhen Polytechnic, Shenzhen 518055, China

DOI:10.1109/JPHOT.2017.2780271

Manuscript received October 25, 2017; revised December 1, 2017; accepted December 2, 2017. Date of publication December 28, 2017; date of current version January 3, 2018. This work was supported in part by the National Natural Science Foundation of China under Grants 61575128, 61425007, 61635007, and 61675037, in part by the Guangdong Natural Science Foundation under Grants 2015A030313541, 2014B050504010, 2015B010105007, 2014A030308007, and 2015A030310243, in part by the Education Department of Guangdong Province under Grant 2015KTSCX119, in part by the Science and Technology Innovation Commission of Shenzhen under Grants JCYJ20160520163134575, JCYJ20160523113602609, JCYJ20160307143501276, JCYJ20160427104925452, and GRCK2016041314562596, and in part by the Development and Reform Commission of Shenzhen Municipality Foundation. *(Feng Zhu and Zhe Zhang contributed equally to this work.)* Corresponding author: Changrui Liao (e-mail: cliao@szu.edu.cn).

Abstract: We demonstrate a phase-shifted fiber Bragg grating with a taper induced by femtosecond laser micromachining. In this configuration, a fiber taper fabricated by an arc discharge in a fiber splicer was sandwiched between two fiber Bragg grating sections, which were formed using femtosecond laser line-by-line inscription. The degree of phase shift produced by this device can be adjusted by introducing axial strain, with a sensitivity of 4.59 pm/$\mu\varepsilon$. A theoretical study was also conducted by modeling the taper under axial strain. The relative deviation between simulated and measured sensitivities is less than 10%.

Index Terms: Fiber Bragg gratings, fiber optics sensors, phase-shift.

1. Introduction

The first phase-shifted fiber Bragg grating (PS-FBG) was introduced in 1990 [1]. It has since been widely used in the fields of all-optical switching [2], wavelength demultiplexing [3], all-optical logic gating [4], optical temporal integration [5], and narrowband fiber filtering [6]. It has also been used to produce tunable wavelength devices [7] and fiber sensors for strain, liquid refractive index, acceleration, and temperature measurements [7]–[12].

Several techniques for fabricating PS-FBGs have been reported in the literature. One common approach employs a phase-shifted phase mask in single exposure [4], [13]–[16]. However, this technique has poor flexibility for changing the grating wavelength. PS-FBGs can be fabricated

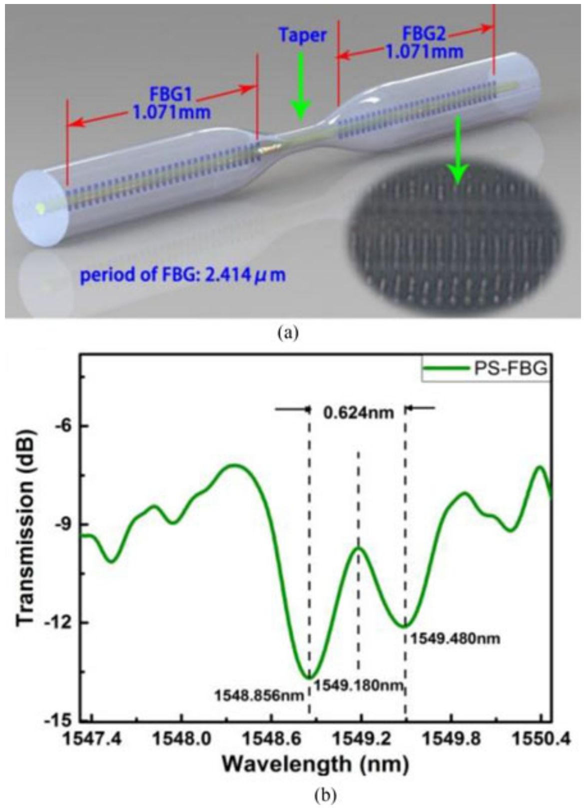

Fig. 1. (a) A schematic diagram of the proposed PS-FBG, with the taper sandwiched between two identical FBGs. (b) The transmission spectrum of one representative PS-FBG.

using the Moire method, a transverse holographic double-exposure technique [17]. The overlaid FBG method [18] is also effective but it requires complex equipment and an exact optical light path. Some authors have attempted to sandwich certain functional structures between two FBGs, i.e., an in-grating bubble [7] fabricated with femtosecond laser-assisted fusion splicing and a microchannel fabricated using either chemical [8]or plasma etching [19]. Although phase shift is tunable for these PS-FBG types, they degrade the integrality of the fiber, which introduces large insertion loss.

In this study, we propose and experimentally demonstrate a novel PS-FBG which includes a taper. Two identical FBGs are inscribed on each side of this taper. Two interesting phenomena have been observed during the axial strain applied to this PS-FBG. First, we found the degree of phase shift in the PS-FBG could be precisely adjusted by varying the axial strain. Secondly, we found the axial-strain sensitivity of the phase-shifted wavelength increased with decreasing taper diameter. A theoretical simulation was also conducted by modeling the taper under axial strain, the results of which were in good agreement with experiment.

2. Device Fabrication

Fig. 1(a) shows a schematic diagram for the proposed PS-FBG, including an inserted optical microscope image of the fabricated FBG. A single-mode fiber (SMF) was first tapered using an arc discharge in a fiber splicer. Two identical FBGs were then inscribed on each side of the taper using femtosecond laser line-by-line inscription. In this manner, the laser point was fixed and the fiber was first translated along the radial direction of the fiber with the intended velocity and distance. After inscription of the first grating pitch, the laser beam was blocked and the fiber was then moved to the starting point of the next grating pitch, after which the cycle was repeated.

TABLE 1
Samples Sizes

Sample Number	Taper Length (μm)	Minimum Fiber Core Diameter (μm)
1	0	9
2	300	4.6
3	480	2.2

Fig. 1(b) shows the transmission spectrum for one representative PS-FBG with a taper length of $\sim$300 μm and a minimum fiber core diameter of $\sim$4.6 μm. During PS-FBG inscription, the pulse energy of the femtosecond laser was attenuated to $\sim$130 n J by rotating a half-wave plate followed by a polarizer. The laser beam was then focused into the fiber core by a 100$\times$ oil objective (NA $=$ 1.25). The pitch of the two FBGs was designated to be 2.412 μm, which corresponds to the 4th Bragg resonant wavelength at $\sim$1550 nm.The length of the two FBGs was 1.071 mm, the length of the laser-inscribed line was set at 15 μm, and the fiber was translated at a speed of 0.15 mm/s in directions perpendicular to the fiber axis. The wavelength of the phase-shifted peak shown in the figure is located at $\sim$1549.180 nm, the full-width minimum is $\sim$0.642 nm, and the insert loss is $\sim$8 dB. The generation of the phase-shifted peak is considered as the result of F-P interference with a pair of FBG reflectors.

3. Axial Strain Measurement

For comparison purposes, three different PS-FBGs were fabricated using this method. Their respective sizes are clearly shown in Table 1. In order to test the axial-strain response of these PS-FBGs, they were fixed between two translation stages with an initial distance of 20 cm. One of the stages was then moved with a step size of 10 μm, corresponding to an axial-strain change of 50 $\mu\varepsilon$ per step [20]. Fig. 2 shows optical microscope images of these three samples and their corresponding transmission spectral evolution with the application of variable axial strain. The phase-shift peak and the FBG resonant dip were each observed to exhibit a significant red shift as the axial strain increased. The red shift of both phase–shift peak and FBG resonant dip is attributed to the elasto-optical effect. Interestingly, in contrast to the PS-FBG without a taper (sample 1), the red-shift amplitude of the phase-shift peak was larger than the FBG resonant dip for a PS-FBG with a taper. As such, significant changes in phase shift can be monitored when a varying amount of axial strain is applied to the PS-FBG with a taper.

Fig. 3 shows experimental data and a linear fit between the wavelength of the phase-shifted peak and the axial strain. The figure also demonstrates that the wavelength of the phase-shifted peak is linearly proportional to changes in the axial strain. The sensitivities of these three samples were measured to be 0.949 pm/$\mu\varepsilon$, 2.37 pm/$\mu\varepsilon$, and 4.59 pm/$\mu\varepsilon$, respectively. The axial strain sensitivity of the phase-shifted peak could be enhanced by decreasing the core diameter.

4. Discussion on the Tunable Phase Shift

When axial strain was applied to this device, an equal load was distributed along each section of the fiber, depending on the local mechanical resistance. The strain loads applied to the tapered and non-tapered areas were equal [20], resulting in the following two equations:

$$\varepsilon_s E A_S = \varepsilon_T E A_T \tag{1}$$

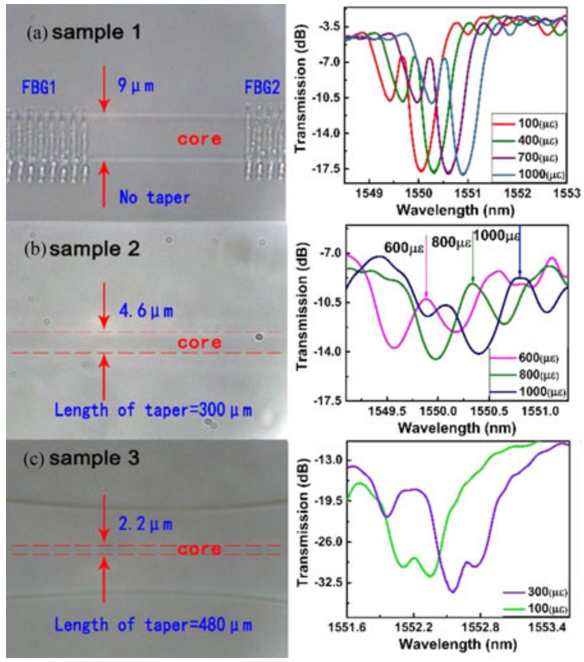

Fig. 2. (a) Optical microscope images and transmission spectral evolution for the first sample, (b) Optical microscope images and transmission spectral evolution for the second sample, (c) Optical microscope images and transmission spectral evolution for the third sample.

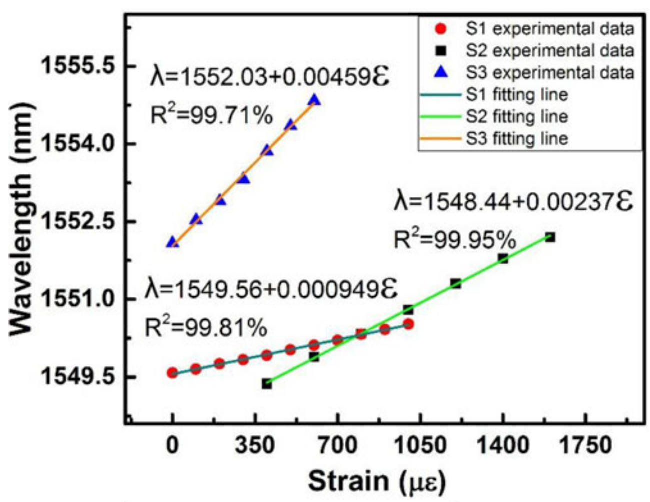

Fig. 3. Experimental data and a fitting relationship between phase-shifted peak wavelength and the axial strain.

Here, ε_S and ε_T represent the axial strain density for the SMF and the taper, A_S and A_T are the cross-sectional area of the SMF and the taper, and E is the elasticity modulus. Obviously, the SMF without a taper has a uniform strain distribution. Fig. 4 demonstrates a simulated distribution of the axial strain density for a tapered fiber using Solidworks. In this simulation, the fiber material is silica, whose elasticity modulus was set to 112,400 N/mm^2, the taper length was 500 μm, and the radius of the un-tapered and tapered areas were 62.5 μm and 15 μm, respectively. The right end was fixed and an axial strain of 10 N was applied to the structure. It can be seen in Fig. 4 that the axial strain was concentrated at the taper area leading to a larger refractive index change due to elasto-optical effect.

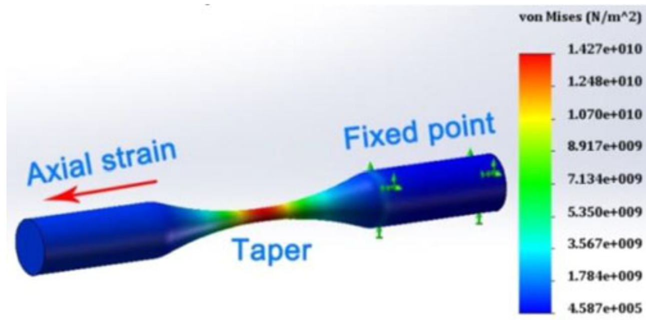

Fig. 4. A simulated distribution of axial strain along the fiber and the axial strain density concentrated in the tapered area.

The presented PS-FBG can be considered as an F-P interferometer (FPI) with a pair of FBG reflectors. The operation wavelength of the FBG and FPI can be expressed as:

$$\lambda_{FBG} = 2n\Lambda \tag{2}$$

$$\lambda_{FPI} = \frac{2nL}{m} \tag{3}$$

where n is the effective refractive index of fiber, Λ is the pitch of FBG, L is the length of F-P cavity (the distance between two FBGs) and m is an integer. Therefore, the axial strain response of λ_{FBG} and λ_{FPI} can be expressed as:

$$\frac{d\lambda_{FBG}}{d\varepsilon} = \frac{\lambda_{FBG}}{n}\frac{dn}{d\varepsilon} \tag{4}$$

$$\frac{d\lambda_{FPI}}{d\varepsilon} = \frac{\lambda_{FPI}}{n}\frac{dn}{d\varepsilon} \tag{5}$$

For the non-tapered configuration, the wavelength change of the phase-shifted peak and the FBG dip are both proportional to $dn/d\varepsilon$ with the same sensitivity of $\lambda dn/\ n d\varepsilon$, where ε is the axial strain. For the tapered configuration in Fig. 4, the refractive index change of the tapered area was larger than that of the surrounding FBG, due to a concentrated axial strain-induced elasto-optical effect. As such, the degree of phase-shift in the PS-FBG can be adjusted by changing the axial strain.

5. Discussion on the Strain Sensitivity

The phaseshift is mainly caused by the refractive index change of the taper when axial strain was applied to this device. Because the wavelength change of the phase-shift peak induced by the given axial strain $\Delta\lambda \propto \Delta n \propto \varepsilon$, we can obtain the following relation:

$$\frac{\frac{d\lambda_T}{d\varepsilon}}{\frac{d\lambda_s}{d\varepsilon}} = \frac{\varepsilon_T}{\varepsilon_S} = \frac{A_S}{A_T} = \frac{r_S^2}{r_T^2} \tag{6}$$

Here, $d\lambda_T/d\varepsilon$ and $d\lambda_s/d\varepsilon$ denote the strain sensitivities of the PS-FBGs with and without a taper, respectively. The relationship between the strain sensitivity and taper radius is demonstrated in Fig. 5.

Because the core diameter of the fiber is gradual along the fiber axis, an equivalent cylinder model was used to replace the taper in the simulation, as shown in Fig. 6.

In this model, circle O_3 is tangent to circle O_1 and the left solid line. Circle O_3 and circle O_4 are asymmetric about the vertical dashed line. From this, we can acquire the profile of the taper, which is marked by the green line. If the radius of the circle O_1 is much larger than that of circle O_3, we can simplify Fig. 6(a) into Fig. 6(b). In Fig. 6(b), |A–D| is the minimum radius of the fiber core, |B–C| is the maximum radius of the fiber core which is equal to the core radius of SMF, and |A–B| is half

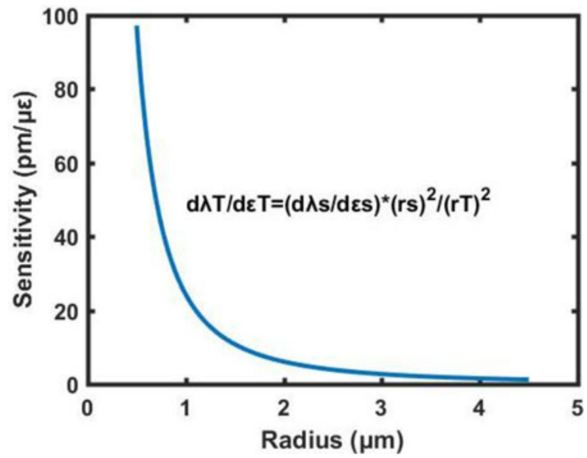

Fig. 5. The relationship between the strain sensitivity and taper radius.

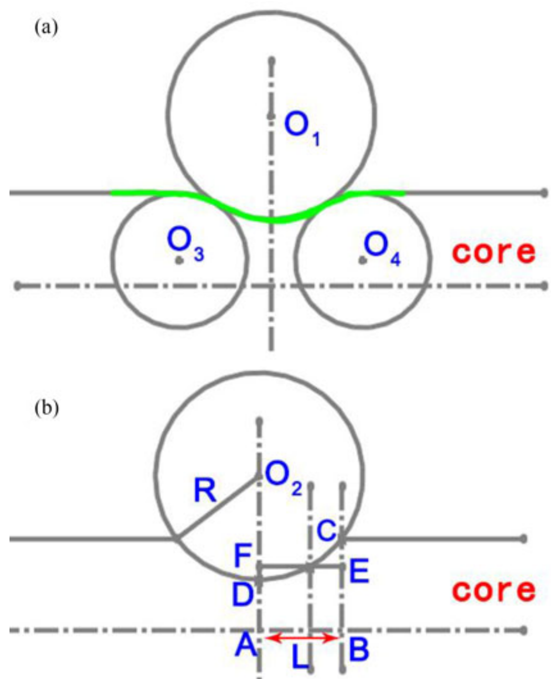

Fig. 6. (a) The equivalent cylinder model of the taper; (b) The simplified model of the taper.

the length of the taper. Theoretically, we can find a rectangle ABEF which has the same area as ABCD. Therefore, the taper could be equivalent to a cylinder with a radius of |A–F| and a length of 2|A–B|. Point A can beset as the origin of the coordinate system, while the right and upward orientations are set to positive. Analytic formula of circle O_2 and the geometric relation in Fig. 6(b) can be expressed as:

$$R^2 = x^2 + (y - R - R_{min})^2 \tag{7}$$

$$R'L = \int_0^L \left(-\sqrt{R^2 - x^2} + R + R_{min}\right) dx \tag{8}$$

$$R^2 = L^2 + (R - R_{max} + R_{min})^2 \tag{9}$$

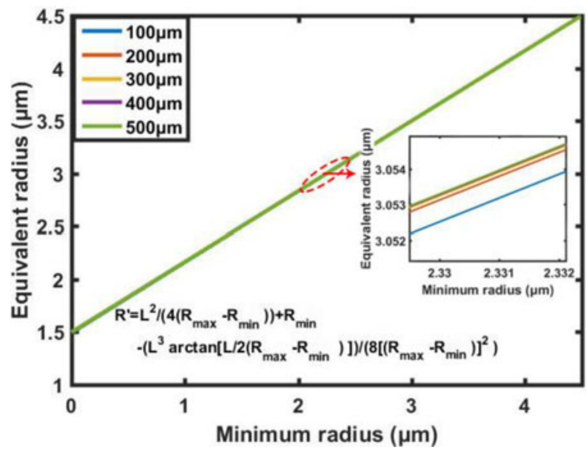

Fig. 7. The relationship between the equivalent radius (R') and the minimum radius ($R_{\min}$) when the taper length is from 100 μm to 500 μm and the inset is the local enlarged image that demonstrates $R_{\min}$ plays a leading role to R'.

Combining (7)–(9), we can obtain the following relation

$$R'L = -\frac{L\sqrt{R^2 - L^2}}{2} - \frac{R^2 \arctan\frac{L}{R}}{2} + L\left(R_{\min} + R\right) \quad (10)$$

Where R is the radius of circle O_2, L is the length of $|A - B|$, R' is the equivalent radius of the tapered core, and R_{max} and R_{min} are the maximum and minimum radius of the tapered core ($R \gg L \gg R_{max} > R_{min}$). After simplification and approximation, the equivalent radius R' can be expressed as:

$$R' = \frac{L^2}{4(R_{\max} - R_{\min})} - \frac{L^3 \arctan\left[\frac{L}{2(R_{\max} - R_{\min})}\right]}{8(R_{\max} - R_{\min})^2} + R_{\min} \quad (11)$$

Fig. 7 shows the relationship between the equivalent radius (R') and the minimum radius (R_{min}) when the taper length is from 100 μm to 500 μm and the inset is the local enlarged image that demonstrates R_{min} plays a leading role to R'. In Fig. 2(b) and (c), taper R' is calculated to be 3.033 μm and 2.233 μm and the sensitivities are calculated to be 2.64 pm/$\mu\varepsilon$ and 4.87 pm/$\mu\varepsilon$ according to (6). Here, the strain sensitivity of the PS-FBGs without a taper is calculated to be 1.21 pm/$\mu\varepsilon$ by use of the method in [21]. The relative deviation between the calculated and measured sensitivities is less than 10%.

6. Conclusion

We have demonstrated a novel PS-FBG induced by femtosecond laser micromachining. A fiber taper was first fabricated using an arc discharge in a fiber splicer and then two FBG sections were fabricated with femtosecond laser line-by-line inscription on both sides of the taper. It was observed that the amount of phase-shift in the PS-FBG could be adjusted by varying the strain and that strain sensitivity could be enhanced by using a thinner taper. An equivalent model for the taper was developed in order to study the theoretical taper strain response with different radii. These calculated results were in excellent agreement with experiment.

References

[1] D. C. J. Reid, C. M. Ragdale, and I. Bennion, "Phase-shifted moire grating fiber resonators," *Electron. Lett.*, vol. 26, pp. 10–12, 1990.

[2] A. Melloni, M. Chinello, and M. Martinelli, "All-optical switching in phase-shifted fiber bragg grating," *IEEE Photon. Technol. Lett.*, vol. 12, no. 1, pp. 42–44, Jan. 2000.

[3] G. P. Agrawal and S. Radic, “Phase-shifted fiber bragg gratings and their application for wavelength demultiplexing,” *IEEE photon. Technol. Lett.*, vol. 6, no. 8, pp. 995–997, Aug. 1994.
[4] Q. Li, J. Song, X. Chen, M. Bi, M. Hu, and S. Li, “All-optical logic gates based on cross phase modulation effect in a phase-shifted grating,” *Appl. Opt.*, vol. 55, pp. 6880–6886, Sep. 2016.
[5] N. Q. Ngo, “Design of an optical temporal integrator based on a phase-shifted fiber Bragg grating in transmission,” *Opt. Lett.*, vol. 32, pp. 3020–3022, 2007.
[6] C. M. Ragdale, D. C. Reid, and D. J. Robbins, “Narrowband fiber grating filters,” *IEEE J. Sel. Areas Commun.*, vol. 8, no. 6, pp. 1146–1150, Aug. 1990.
[7] C. R. Liao *et al.*, “Tunable phase-shifted fiber bragg grating based on femtosecond laser fabricated in-grating bubble,” *Opt Lett.*, vol. 38, pp. 4473–4476, Nov. 2013.
[8] K. M. Zhou, Z. Z. Yan, and L. Zhang, “Refractometer based on fiber bragg grating Fabry-Pérot cavity embedded with a narrow microchannel,” *Opt. Exp.*, vol. 19, pp. 11769–11779, 2011.
[9] T. Yoshino, Y. Sano, and D. Ota, “Fiber-Bragg-grating based single axial mode fabry-perot interferometer and its strain and acceleration sensing applications,” *J. Lightw. Technol.*, vol. 34, no. 9, pp. 2241–2250, May 2016.
[10] C. M. Jewart, Q. Wang, and J. Canning, “Ultrafast femtosecond-laser-induced fiber Bragg gratings in air-hole microstructured fibers for high-temperature pressure sensing,” *Opt. Lett.*, vol. 35, pp. 1443–1445, 2010.
[11] A. Iadicicco, A. Cusano, and S. Campopiano, “Thinned fiber Bragg gratings as refractive index sensors,” *IEEE Sensors J.*, vol. 5, no. 6, pp. 1288–1295, Dec. 2005.
[12] Z. Zhang *et al.*, “Hollow-core-fiber-based interferometer for high-temperature measurements,” *IEEE Photon. J.*, vol. 9, no. 2, Apr. 2017, Art. no. 7101109.
[13] R. Kashyap, P. F. Mckee, and D. Armes, “UV written reflection grating structures in photosensitive optical fibers using phase-shifted phase masks,” *Electron. Lett.*, vol. 30, pp. 1977–1978, 1994.
[14] J. He *et al.*, “Highly birefringent phase-shifted fiber bragg gratings inscribed with femtosecond laser,” *Opt. Lett.*, vol. 40, pp. 2008–2011, May 2015.
[15] D. Gatti, G. Galzerano, and D. Janner, “Fiber strain sensor based on a π-phase-shifted bragg grating and the pound-drever-hall technique,” *Opt. Exp.*, vol. 16, pp. 1945–1950, 2008.
[16] G. Curatu, S. Larochelle, C. Pareeacute;, and P. A. Beeacute;langer, “Antisymmetric pulse generation using phase-shifted fiber bragg grating,” *Electron. Lett.*, vol. 38, pp. 307–309, 2002.
[17] L. Zhao, L. Li, A. P. Luo, J. Z. Xia, R. H.Q, and Z. J. Fang, “Bandwidth controllable transmission filter based on moiré fiber Bragg grating,” *Optik*, vol. 113, pp. 464–468, 2002.
[18] A. Shamir and A. A. Ishaaya, “Femtosecond inscription of phase-shifted gratings by overlaid fiber bragg gratings,” *Opt Lett.*, vol. 41, pp. 2017–2020, May 2016.
[19] H. Kumazaki, Y. Yamada, and H. Nakamura, “Tunable wavelength filter using a Bragg grating fiber thinned by plasma etching,” *IEEE Photon. Technol. Lett.*, vol. 13, no. 11, pp. 1206–1208, Nov. 2001.
[20] C. R. Liao, D. N. Wang, and Y. Wang, “Microfiber in-line mach–zehnder interferometer for strain sensing,” *Opt. Lett.*, vol. 38, pp. 757–759, 2013.
[21] X. F. Zhou, J. F. Xu, and L. Liang, “Design and analysis of fiber bragg grating cable tension sensor,” *Chin. J. Sens. Actuators*, vol. 20, pp. 1007–1011, 2007.